RSC Advances




ROYAL SOCIETY OF CHEMISTRY

www.rsc.org/advances

Journal Name

COMMUNICATION

# The Closed-Environment CVD Method for preparing three-dimensional defect controllable Graphene Foam with conductive interconnected network for Lithium-ion Battery application

Received 00th January 20xx,
Accepted 00th January 20xx

DOI: 10.1039/x0xx00000x

www.rsc.org/

W. X. Wang,[a] S. C. Zhang, *[a] Y. L. Xing,[a] S. B. Wang[a] and Y. B. Ren[a]

**A 3D defect controllable graphene foam (GF) with conductive interconnected network is prepared by a CVD process in a chosed environment, which we refer to as the closed-environment CVD method. The resulting GF not only is high quality, but also is provided with controllable defect density, offering a great potential in Lithium-ion batteries (LIBs) application. When ZnO anchored on the 3D GF to construct ZnO/GF composite as anode for LIBs, benefiting from the advantages of graphene and unique structural features, it exhibits a high reversible capacity of 851.5 mA h $g^{-1}$ at 0.2 A $g^{-1}$, good cycling performance and excellent rate capability. Notably, the higher defect density of GF leads to an increase in the capacity of ZnO/GF, meanwhile, it maintains an excellent rate performance.**

The ever-increasing energy demand driven by rapid development of portable electronic devices, renewable energy products, and electric vehicles, is one of the key issues in the modern world. To address the challenge, high-effective and environment-friendly devices for energy conversion and storage are required. Lithium-ion batteries (LIBs) with high energy density and long cycle life, is regarded as one of the most promising representatives of the main power source. However, commercial LIBs anode material graphite with limited reversible capacity (theoretical capacity is 372 mA h $g^{-1}$) is an obstacle to the development of high performance LIBs. Zinc oxide (ZnO) with high theoretical specific capacity, environment friendly and low cost is a promising material for LIBs anode. Unfortunately, ZnO is still hindered by its poor electrical conductivity and tremendous volume changes during charge/discharge process, leading to a capacity fading upon cycling and poor rate capability. [1, 2]

Graphene, a two-dimensional (2D) monolayer of carbon atoms, with the unique properties of giant theoretical specific surface area (2630 $m^2$ $g^{-1}$), extremely high electric/thermal conductivity, extraordinary flexibility, and chemical stability[3-9] offers a promising approach to realize highly efficient LIBs. Currently, considerable efforts have been devoted into combining graphene with metal oxides, which is a valued strategy to maximize the advantages of both material. [10-14]

Usually, the success of graphene applications for LIBs is largely dependent on the properties of graphene, such as high quality improving the conductivity of active materials and large specific surface area increasing the contact area between active material and electrolyte.[12-18] The graphene preparation method plays a crucial role in determining the properties of the final product. Versatile methods have been developed for the preparation of graphene, such as liquid phase exfoliation,[19-21] reduction of graphene oxide,[22, 23] and chemical vapor deposition (CVD),[24-26] etc. Owing to the ease of processing, chemically derived graphene sheets are widely employed in LIBs. However, these graphene sheets are hindered by the large number of defects introduced during preparation process and/or high inter-sheet contact resistance in a 3D structure. Although the defect-free high-quality graphene has been grown by CVD, the defect in graphene sheet still plays an important role in LIBs, which provides additional active sites for lithium storage, facilitates graphene integration with other materials, enables lithium diffusion and prevents lithium clustering. [17, 27] Obviously, overmuch defects in graphene sheet will destroy electrical conductivity and mechanical robustness. Therefore, development of an efficient method for preparing 3D high quality graphene with controllable defect density is critical for its application in LIBs.

Here, we report the preparation of 3D defect controllable GF with conductive interconnected network via closed-environment CVD method, in which carbon source PMMA reacts with hydrogen in a closed-environment at 1000 °C, and then graphene form on Ni foam. The resulting GF not only is relatively high quality, but also is provided with controllable defect density. Moreover, changing PMMA quantity can simply and effectively control the defect density. Even with a large

[a] School of Materials Science and Engineering, Beihang University, Beijing 100191, PR China. E-mail: csc@buaa.edu.cn (S. Zhang). Tel.: +86 01082339319; fax: +86 01082338148.

†Electronic Supplementary Information (ESI) available: Experimental details, SEM and XRD. See DOI: 10.1039/x0xx00000x

Journal Name

COMMUNICATION

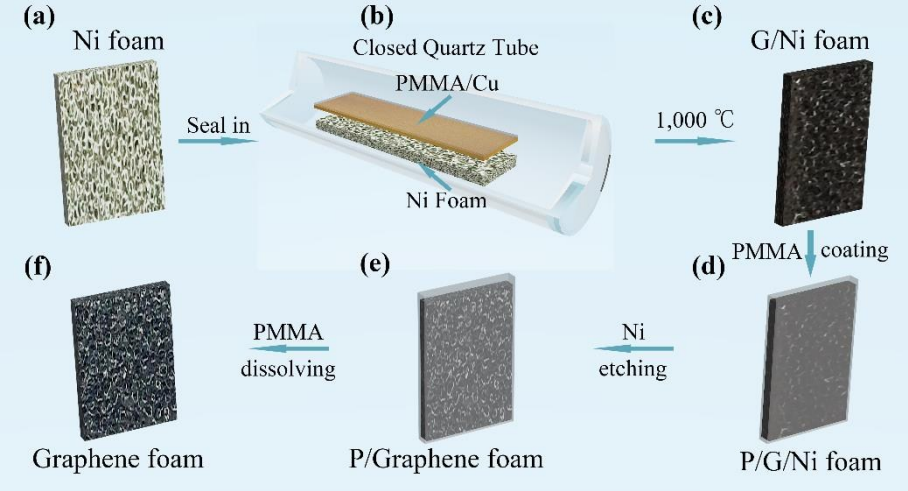


**Fig.1** Schematic illustration of synthesis process of 3D free-standing GF. (a-c) closed-environment CVD method growth of graphene on Ni foam by using the sealed quartz tube, as shown in (b). (d) G/Ni foam coat with thin layer PMMA film. (e) G/Ni foam etch Ni foam with PMMA protected. (f) free-standing GF after dissolving the thin PMMA layer with hot acetone.

quantity of PMMA, the quality and electrical conductivity of graphene are still better than that of chemically derived graphene. The 3D GF is employed to construct graphene/zinc oxide (ZnO/GF) composite as anode for LIBs. In this unique structure, the GF directly grow on current collector Ni foam, providing compact electrical contact between GF and current collector for fast electron transfer from active materials to current collector via underlying GF. Moreover, the conductive interconnected 3D GF increase the effective contact area between ZnO particles and electrolyte, providing more diffusion channel between Li-ion and ZnO particle. Consequently, the ZnO/GF composite exhibits a high reversible specific capacity of ~851.5 mA h $g^{-1}$ at a current density of 0.2 A $g^{-1}$ even after 200 cycles and an excellent rate performance. Notably, if GF with higher defect density were employed to prepare ZnO/GF, the specific capacity of electrode is improved, meanwhile, and the excellent rate performance is retained.

The process of synthesis 3D GF by the closed-environment CVD is illustrated in Fig. 1. In this method, we seal template Ni foam and solid carbon sources PMMA with hydrogen in a closed quartz tube (Fig. 1b and Fig. S1†) to prepare graphene at 1000 $^{o}$C for 20min (Fig. 1a and c). Different from the general CVD method, which produce graphene in an open environment with flowing $H_2$ and carbon source, in our method, PMMA/Cu films react with $H_2$ in a closed environment In this experiment, GFs were prepared with a series of PMMA quantity: from 200μl to 700μl, the sample referred to as GF200 to GF700. To obtain 3D GF with intact structure, a thin layer of PMMA was coated on G/Ni foam by drop-coating. This layer of PMMA prevented the 3D GF from collapsing during nickel etching (Fig. 1d and e). After etching nickel process, the layer of PMMA was dissolved by hot acetone, then a monolith of interconnected foam-like 3D graphene was obtained (Fig. 1f).

The 3D GF inherits and maintains the 3D continuous foam-like structure of Ni foam without any severe structural collapse

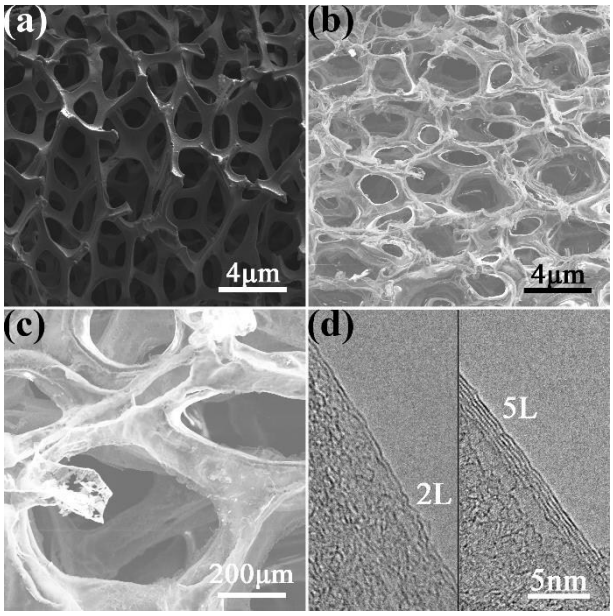


**Fig. 2** SEM images of (a) G/Ni foam after closed-environment CVD, (b and c) 3D GF after removal of Ni foam. (d) High-resolution TEM image of the edge of a graphene sheet, the interlayer spacing of bilayer (2L) and five-layer (5L) graphene is~0.33nm.The sample was prepared with a PMMA quantity of 300μl.

Journal Name

COMMUNICATION

(Figs. 2b and c). The ripples and wrinkles are formed on the graphene film during the cooling process (Fig. S2), because of the different thermal expansion coefficient between nickel and graphene. [28] Moreover, the ripples and wrinkles cross the grain boundary of nickel, indicating the 3D GF is composed of interconnected graphene sheets. This structure eliminates contact resistance between graphene sheets, enhances the electrical conductivity of entire 3D GF. The 3D GF consist of bi- to few-layer graphene sheets, as shown in high-resolution TEM image (Fig. 2d). The non-uniformity is attributed to the each grain boundaries in polycrystalline Ni foam, which have the independent effect on graphene growth.[29] Raman spectra of 3D GF presents a typical spectra of few-layer graphene (Fig. 3a),[30] which is consistent with the average layer number of graphene derived from specific area (detail in supplementary information) (Fig. 3b). In addition, the specific area and electrical conductivity of GF is up to ~652.4 $m^2$ $g^{-1}$ and ~2.8 S $cm^{-1}$ respectively, corresponding to a PMMA quantity of 200µl (Fig. 3a and S3).

The 3D GF is provided with controllable defect density. In order to control the defect density, we changed the quantity of carbon source PMMA in closed-environment CVD. In Raman spectra of graphene, D band is related to the disorder and defect in graphene, G band represents the carbon $sp^2$ bonding,[31] therefore, we define defect density as the intensity ratio between the D bands and G bands ($I_D/I_G$). The GF200 with suppressed D band gives a high $I_D/I_G$ ratio of ~0.10. The ratio increase along with PMMA quantity, suggesting higher PMMA quantity leads to an increase in the number of defect density. In addition to Raman spectra, XPS was also employed to characterize 3D GF. The High resolution C (1s) spectrum is subdivided into three peaks representing different binding state: carbon $sp^2$ bonding (C-C, ~284.7 eV), epoxide/hydroxyl groups (C-O, ~285.3 eV) and carbonyl groups (C=O, ~288.0 eV) (Fig. 3c and d).[32] This result indicates the 3D GF exists O-containing defect (C-O and C=O). In contrast to C-C peak, the intensity of C-O peak increases with a higher PMMA quantity. Therefore, the intensity ratio between the defect peak (C-O and C=O) and total peak can be used to measure the number of O-containing defect in graphene (Table. S1). As a result, the O-containing defect content of GF300 and GF500 are ~28% and ~37% respectively, indicating the increase of defect is caused by higher PMMA quantity. This result could be mainly due to the

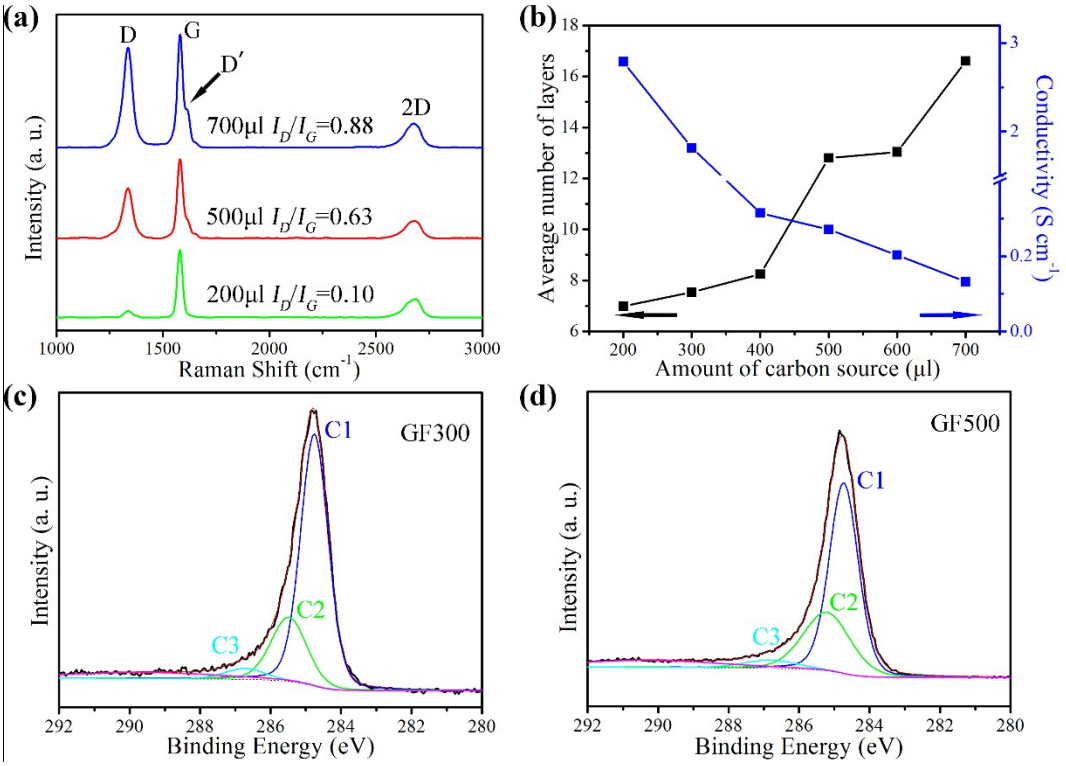


**Fig. 3** (a) Raman spectra of 3D GF. The GF were prepared with the amount of PMMA solution of 200µl, 500µl, and 700µl. (b) Average number of graphene layers in 3D GF as a function of the amount of carbon source PMMA used in closed-CVD growth. (c and d) Decomposition of the high-resolution XPS spectra of the C1s regions for G/Ni foam with C1 (C-C), C2 (C-O), C3 (C=O). The samples were prepared with PMMA solution 300µl and 500µl, respectively.

Journal Name

COMMUNICATION

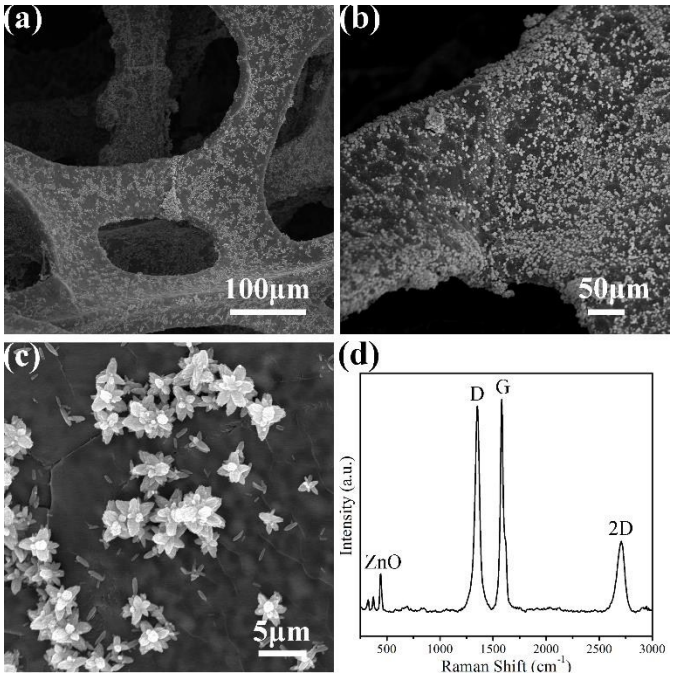


**Fig. 4** (a-c) SEM images of ZnO/GF composite with different magnification. (d) Raman spectra of ZnO/GF composite

pyrolysis intermediates continuous accumulation and participation in the formation of graphene. Generally, there are two kinds of formation mechanism in the graphene growth on nickel: the deposition mechanism during the reacting process and segregation/precipitation mechanism during the cooling process.[33-35] In a closed environment, the incomplete decomposition intermediates resulting from the pyrolysis of PMMA, under the influence of the deposition mechanism, directly deposit to form graphene, because those intermediates can not be promptly removed from the reaction system. Therefore, when using a higher PMMA quantity in closed reaction system, the concentration of intermediate increases, which results in an increase in the defect density of graphene. In addition to, the electrical conductivity of GF reduce with the PMMA quantity increasing (Fig. 3b). Because the electrical conductivity of graphene is strongly depend on the π network,[5] which is impaired by the increased number of defects.

Constructing a graphene/metal oxides composite is important to improve the electrochemical performance of metal oxide anode materials. The 3D GF was employed to fabricate ZnO/graphene foam (ZnO/GF) composite as anode for LIBs. The morphology of the resulting ZnO/GF shows flower-like ZnO particles uniformly disperse on graphene film, this structure can accommodate the volume changes of ZnO particles during the lithiation/delithiation process (Fig. 4b). Besides characteristic band of graphene, the Raman spectra of ZnO/GF contains a sharp peak at ~430 $cm^{-1}$ (Fig. 4a), which is attributed to ZnO $E_2$ phonon mode, indicating the existence of Zinc Oxide.[36]

The electrochemical properties of ZnO/GF were investigated. The ZnO/GF was directly employed as the work electrode without the conductive carbon black and binder. The electrochemical performance behaviours of the ZnO/GF anodes were tested by cyclic voltammetry (CV), the resulting CV curves recorded in the first three cycles at a scan rate of 0.1 mV $s^{-1}$ within a voltage window of 0.01-3.0 V (vs. $Li^+/Li$) are shown in Fig. 5a. The CV curves almost overlap after the first cycle, indicating the excellent electrochemical stability of ZnO/GF electrode during the process of lithiation/delithiation. In the first cathodic cycle, the wide peak at 0.75-1.25 V is attributed to two electrochemical reactions, including the reduction of ZnO into Zn and Zn alloying with Li to formation of $Zn_xLi_y$.[37] A sharp peak at 0.25 V is caused by the electrolyte decomposition and the formation of solid electrolyte interphase (SEI) film, which disappears in the following cycles. A reversible peak at 0.1 V corresponds to the intercalation of Li into the graphene layers. In first anodic cycle, the first peak at 0.1 V is ascribed to the Li deintercalation from graphene layers. The wide peak at 1.0-1.75 V is caused by the process of $Zn_xLi_y$ multistep dealloying. And the last peak at 2.25 V corresponds to the reversible conversion reaction between Zn and ZnO, indicating a high capacity and stable cycle property. To identify the discharge voltage plateau position and capacity, the charge-discharge voltage profiles of the ZnO/GF electrode acquired at a current density of 0.2 A $g^{-1}$ within a voltage window of 0.01-3.0 V (vs. $Li^+/Li$) for the first three cycles (Fig. 5b). Obviously, the plateaus on the charge-discharge voltage profiles are consistent with the CV curves. The ZnO/GF electrode exhibits initial discharge and charge capacities of 1658 mA h $g^{-1}$ and 1124 mA h $g^{-1}$ respectively, corresponding to a relative lower initial Coulombic efficiency of 67.8%, which is caused by the electrolyte decomposition and SEI film formation. According to previous reports,[38,39] the irreversible capacity loss in the first two cycles can be attributed to the formation of SEI film.

In order to demonstrate the effect of different defect density on the electrochemical properties of ZnO/GF, the ZnO/GF electrodes prepared with the GF300 and GF500 were employed to characterize the cycling and rate performance, the resulting electrodes were referred as ZnO/GF300 and ZnO/GF500. Both electrodes exhibit high capacity and good cycle performance (Fig. 5c). After 200 charge−discharge cycles, the ZnO/GF500 and ZnO/GF300 still demonstrate a lithium storage capacity of ~851.5 mAh $g^{-1}$ and 601 mAh $g^{-1}$. Although a relatively low

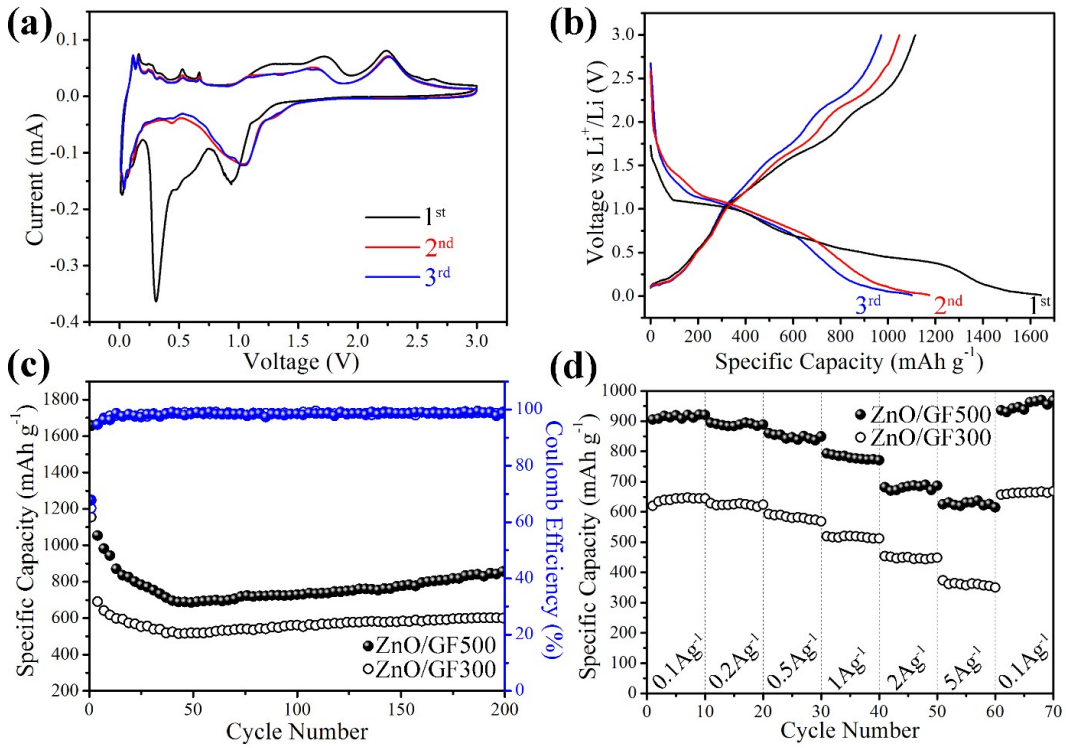


Fig. 5 The electrochemical performance of the ZnO/GF electrode: (a) CV curves of the ZnO/GF between 0.01 and 3.0 V at a scanning rate of 0.1 mV $s^{-1}$; (b) charge-discharge profiles of the ZnO/GF electrode at 1st, 2nd and 3rd cycles between 0.01 and 3.0V with current density of 0.2 A $g^{-1}$; (c) cycling performance of ZnO/GF electrodes with different defect density at a current density of 0.2 A $g^{-1}$; (d) rate performance of electrodes at different current densities from 0.1 A $g^{-1}$ to 5 A $g^{-1}$ in the voltage range of 0.01-3.0V.

coulombic efficiency is observed for each electrode, after few cycles, the coulombic efficiency reaches over 98%. Compared with ZnO/GF300, ZnO/GF500 with higher defect density in GF shows a larger specific capacity. This result mainly could be ascribed to the structural defect in graphene, which plays a role of reversible lithium storage site during charge-discharge process.[40] Therefore, the higher defect density in GF contributes the larger additional capacity. In addition to additional active sites, GF500 with higher defect density leads to an increase of ZnO content in ZnO/GF composite, improving the areal capacity (Fig. S5). The content of ZnO in ZnO/GF electrode is ~71.1wt% and ~80.0wt% for ZnO/GF300 and ZnO/GF500 respectively.

The rate performance with a series of current densities from 0.1 A $g^{-1}$ to 5A $g^{-1}$ were examined (Fig. 5d). It is clearly that both electrode delivers a satisfactory reversible capacity at each current density. Even at a current density as high as 5 A $g^{-1}$, ZnO/GF500 and ZnO/GF300 maintain a reversible capacity of 615.2 mAh $g^{-1}$ and 349.6 mAh $g^{-1}$, corresponding to ~69% and ~56% of the capacity (920.5 mA h $g^{-1}$ and 643.9 mA h $g^{-1}$) obtained at 0.1 A $g^{-1}$respectively. The discharge capacities of both electrodes remain stable with a reasonable decrease, suggesting a rapid charge transport process of the electrodes. Furthermore, it is should be noticed that the capacities of electrodes are restored after 60 cycles upon returning the current density to 0.1 A $g^{-1}$, indicating a great cycling stability at high rates. Notably, although the ZnO/GF500 is provided with higher defect density, it presents excellent rate capability and cycling stability. This result suggests that the fast charge transport channel still be provided by GF500 to improve the rate performance of ZnO/GF electrode. c

High reversible capacity, good cycling performance, and excellent rate capability of ZnO/GF electrode can be attributed to several reasons. First, the 3D GF direct growth on current collector of Ni foam can host ZnO particles, which works as a highly conductive matrix for good electrical contact between ZnO particles and current collector, offering fast transport channels for charge carriers. Second, the 3D conductive interconnected graphene network with large surface area allows more ZnO particles to contact with the electrolyte, providing more diffusion paths for Li ion to transport to ZnO particles. Third, the macroscopically porous structure in 3D GF is favorable for electrolyte access.

## Conclusions

In summary, the 3D defect controllable GF with conductive interconnected network was prepared by the closed-environment CVD method. Besides the high quality, the 3D GF is provided with controllable defect. It is demonstrated that the defect density of 3D GF can directly be changed by adjusting PMMA quantity. When the 3D GF is employed to fabricate ZnO/GF composite for LIBs anode, it exhibits a high specific capacity of 851.5 mA h $g^{-1}$ after 200 cycles, good cycling stability

and excellent rate performance. It is worth to notice that the higher defect density of GF combining with ZnO, the specific capacity of ZnO/GF electrode is promoted, at same time, and the excellent rate performance is retained. In principle, the closed-environment CVD method offers a novel way to prepare graphene materials with controllable defect density and desired heteroatom by changing the type and quantity of carbon source, such as B, N, and S. We believe that the 3D GF with specific heteroatom and controllable density would be a great promising material in energy storage application.

## Acknowledgements

This work was supported by the National Basic Research Program of China (973 Program) (2013CB934001), National Natural Science Foundation of China (51274017), National 863 Program of China (2012AA052201 and 2012AA110102), and International S&T Cooperation Program of China (2012DFR60530).

## Notes and references

1 M. V. Reddy, G. V. Subba Rao and B. V. Chowdari, *Chemical reviews*, 2013, **113**, 5364-5457.
2 Z. Zhou, K. Zhang, J. Liu, H. Peng and G. Li, *Journal of Power Sources*, 2015, **285**, 406-412.
3 A. K. Geim and K. S. Novoselov, *Nature materials*, 2007, **6**, 183-191.
4 A. K. Geim, *Science*, 2009, **324**, 1530-1534.
5 K. S. Novoselov, A. K. Geim, S. V. Morozov, D. Jiang, Y. Zhang, S. V. Dubonos, I. V. Grigorieva and A. A. Firsov, *Science*, 2004, **306**, 666-669.
6 K. S. Novoselov, A. K. Geim, S. V. Morozov, D. Jiang, M. I. Katsnelson, I. V. Grigorieva, S. V. Dubonos and A. A. Firsov, *Nature*, 2005, **438**, 197-200.
7 Y. Zhang, Y. W. Tan, H. L. Stormer and P. Kim, *Nature*, 2005, **438**, 201-204.
8 A. A. Balandin, S. Ghosh, W. Z. Bao, I. Calizo, D. Teweldebrhan, F. Miao and C. N. Lau, *Nano letters*, 2008, **8**, 902-907.
9 C. Lee, X. D. Wei, J. W. Kysar and J. Hone, *Science*, 2008, **321**, 385-388.
10 S. Yang, X. Feng, S. Ivanovici and K. Mullen, *Angewandte Chemie*, 2010, **49**, 8408-8411.
11 E. Yoo, J. Kim, E. Hosono, H. Zhou, T. Kudo and I. Honma, *Nano letters*, 2008, **8**, 2277-2282.
12 H. Wang, Y. Yang, Y. Liang, L. F. Cui, H. S. Casalongue, Y. Li, G. Hong, Y. Cui and H. Dai, *Angewandte Chemie*, 2011, **50**, 7364-7368.
13 W.-Y. Tsai, R. Lin, S. Murali, L. Li Zhang, J. K. McDonough, R. S. Ruoff, P.-L. Taberna, Y. Gogotsi and P. Simon, *Nano Energy*, 2013, **2**, 403-411.
14 Y. Tao, X. Xie, W. Lv, D.-M. Tang, D. Kong, Z. Huang, H. Nishihara, T. Ishii, B. Li, D. Golberg, F. Kang, T. Kyotani and Q.-H. Yang, *Sci Rep-Uk*, 2013, **3**.
15 J. Zhu, D. Yang, Z. Yin, Q. Yan and H. Zhang, *Small*, 2014, **10**, 3480-3498.
16 R. Raccichini, A. Varzi, S. Passerini and B. Scrosati, *Nature materials*, 2015, **14**, 271-279.
17 K. Chen, S. Song, F. Liu and D. Xue, *Chemical Society reviews*, 2015, **44**, 6230-6257.
18 F. Bonaccorso, L. Colombo, G. Yu, M. Stoller, V. Tozzini, A. C. Ferrari, R. S. Ruoff and V. Pellegrini, *Science*, 2015, **347**, 1246501.
19 D. Wei, L. Grande, V. Chundi, R. White, C. Bower, P. Andrew and T. Ryhanen, *Chem Commun (Camb)*, 2012, **48**, 1239-1241.
20 M. Cai, D. Thorpe, D. H. Adamson and H. C. Schniepp, *Journal of Materials Chemistry*, 2012, **22**, 24992.
21 K. R. Paton, E. Varrla, C. Backes, R. J. Smith, U. Khan, A. O'Neill, C. Boland, M. Lotya, O. M. Istrate, P. King, T. Higgins, S. Barwich, P. May, P. Puczkarski, I. Ahmed, M. Moebius, H. Pettersson, E. Long, J. Coelho, S. E. O'Brien, E. K. McGuire, B. M. Sanchez, G. S. Duesberg, N. McEvoy, T. J. Pennycook, C. Downing, A. Crossley, V. Nicolosi and J. N. Coleman, *Nature materials*, 2014, **13**, 624-630.
22 W. S. H. Jr and R. E. Offeman, 1958, 1339.
23 S. Park and R. S. Ruoff, *Nature nanotechnology*, 2009, **4**, 217-224.
24 X. Li, W. Cai, J. An, S. Kim, J. Nah, D. Yang, R. Piner, A. Velamakanni, I. Jung, E. Tutuc, S. K. Banerjee, L. Colombo and R. S. Ruoff, *Science*, 2009, **324**, 1312-1314.
25 X. Li, C. W. Magnuson, A. Venugopal, J. An, J. W. Suk, B. Han, M. Borysiak, W. Cai, A. Velamakanni, Y. Zhu, L. Fu, E. M. Vogel, E. Voelkl, L. Colombo and R. S. Ruoff, *Nano letters*, 2010, **10**, 4328-4334.
26 L. Gao, W. Ren, J. Zhao, L.-P. Ma, Z. Chen and H.-M. Cheng, *Applied Physics Letters*, 2010, **97**, 183109.
27 F. Yao, F. Guenes, T. Huy Quang, S. M. Lee, S. J. Chae, K. Y. Sheem, C. S. Cojocaru, S. S. Xie and Y. H. Lee, *Journal of the American Chemical Society*, 2012, **134**, 8646-8654.
28 S. J. Chae, F. Güneş, K. K. Kim, E. S. Kim, G. H. Han, S. M. Kim, H.-J. Shin, S.-M. Yoon, J.-Y. Choi, M. H. Park, C. W. Yang, D. Pribat and Y. H. Lee, *Advanced materials*, 2009, **21**, 2328-2333.
29 Y. Zhang, L. Gomez, F. N. Ishikawa, A. Madaria, K. Ryu, C. A. Wang, A. Badmaev and C. W. Zhou, *J Phys Chem Lett*, 2010, **1**, 3101-3107.
30 M. S. Dresselhaus, A. Jorio, M. Hofmann, G. Dresselhaus and R. Saito, *Nano letters*, 2010, **10**, 751-758.
31 A. C. Ferrari and D. M. Basko, *Nature nanotechnology*, 2013, **8**, 235-246.
32 I. Bertóti, M. Mohai and K. László, *Carbon*, 2015, **84**, 185-196.
33 X. Li, W. Cai, L. Colombo and R. S. Ruoff, *Nano letters*, 2009, **9**, 4268-4272.
34 S. Kumar, N. McEvoy, T. Lutz, G. P. Keeley, V. Nicolosi, C. P. Murray, W. J. Blau and G. S. Duesberg, *Chem Commun (Camb)*, 2010, **46**, 1422-1424.
35 M. Sarno, C. Cirillo, R. Piscitelli and P. Ciambelli, *Journal of Molecular Catalysis A: Chemical*, 2013, **366**, 303-314.
36 N. Ashkenov, B. N. Mbenkum, C. Bundesmann, V. Riede, M. Lorenz, D. Spemann, E. M. Kaidashev, A. Kasic, M. Schubert, M. Grundmann, G. Wagner, H. Neumann, V. Darakchieva, H. Arwin and B. Monemar, *J Appl Phys*, 2003, **93**, 126.
37 N. Li, S. X. Jin, Q. Y. Liao and C. X. Wang, *ACS Appl Mater Interfaces*, 2014, **6**, 20590-20596.
38 M. Ahmad, S. Yingying, A. Nisar, H. Sun, W. Shen, M. Wei and J. Zhu, *Journal of Materials Chemistry*, 2011, **21**, 7723.
39 S. B. Wang, Y. B. Ren, G. R. Liu, Y. L. Xing and S. C. Zhang, *Nanoscale*, 2014, **6**, 3508-3512.
40 D. Pan, S. Wang, B. Zhao, M. Wu, H. Zhang, Y. Wang and Z. Jiao, *Chemistry of Materials*, 2009, **21**, 3136-3142.



 

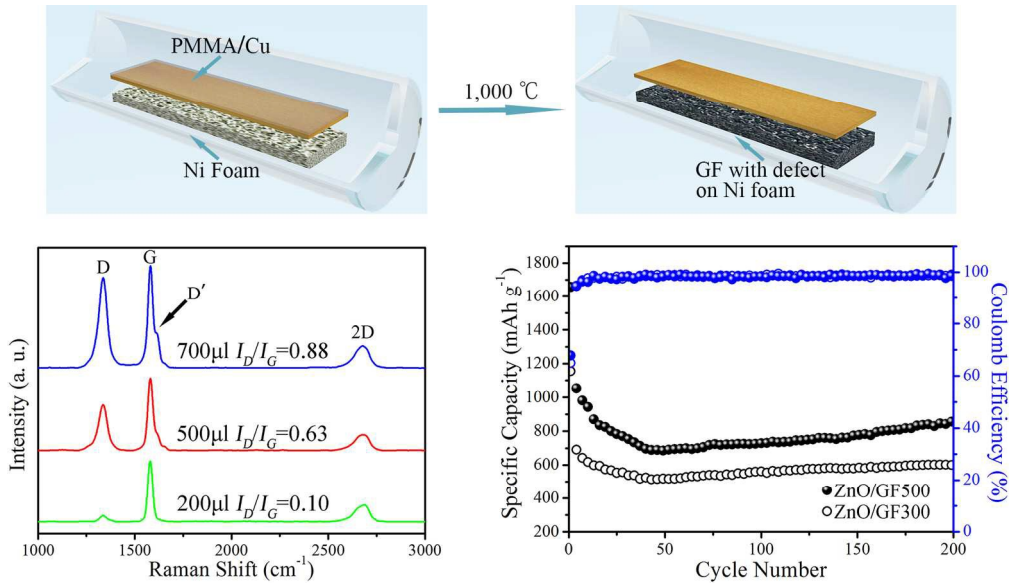


682x393mm (72 x 72 DPI)